

WX Cen (\equiv WR 48c) – a possible type Ia Supernova progenitor^{*}

A. S. Oliveira [†], and J. E. Steiner

Instituto de Astronomia, Geofísica e Ciências Atmosféricas - IAG, Universidade de São Paulo, CP 9638, 01065-970, São Paulo, Brazil

Accepted ?????. Received ????; in original form ????

ABSTRACT

We confirm the orbital period of WX Cen \equiv WR 48c determined by Diaz & Steiner (1995) – DS95 – and refined its value to $P_{orb} = 0.416\,961\,5(\pm 22)$ d. The light curve of this object has a peak to peak variation of approximately 0.32 magnitudes. It is non-sinusoidal in the sense that it has a V-shaped narrow minimum, similar to the ones seen in V Sge, V617 Sgr and in Compact Binary Supersoft Sources – CBSS.

Most of the emission lines in the optical spectrum are due to Balmer, He II, C IV, N V, O V and O VI. An analysis of the He II Pickering series decrement shows that the system has significant amount of hydrogen. The emission lines of He II 4686Å became weaker between the 1991 and 2000/2002 observations, indicating distinct levels of activity. The spectra of WX Cen show variable absorption features in the Balmer lines with $V = -2900$ km s⁻¹ and in emission with $V = \pm 3500$ km s⁻¹. These highly variable events remind the satellites in emission of CBSS.

We estimate the color excess as $E(B - V) = 0.63$ on the basis of the observed diffuse interstellar band at 5780Å. Given the distance-color excess relation in the direction of WX Cen, this implies a distance of 2.8 ± 0.3 kpc. Interstellar absorption of the Na I D lines show components at -4.1 km s⁻¹, which corresponds to the velocity of the Coalsack, and three other components at -23.9 , -32.0 and -39.0 km s⁻¹. These components are also seen with similar strengths in field stars that have distances between 1.8 and 2.7 kpc. The intrinsic color of WX Cen is $(B - V)_0 = -0.2$ and the absolute magnitude, $M_V = -0.5$.

Extended red wings in the strong emission lines are seen. A possible explanation is that the system has a spill-over stream similar to what is seen in V617 Sgr. We predict that when observed in opposite phase, blue wings would be observed. A puzzling feature that remains to be explained is the highly variable red wing ($V \sim 700$ km s⁻¹) of the O VI emission lines as well as of the red wings of the H and He lines.

The velocity of the satellite-like feature is consistent with the idea that the central star is a white dwarf with a mass of $M \sim 0.9M_{\odot}$. With the high accretion rate under consideration, the star may become a SN Ia in a time-scale of 5×10^6 years.

Key words: stars: individual: WX Cen – stars: binaries: close – stars: emission-line.

1 INTRODUCTION

WX Cen was initially identified by Eggen, Freeman & Sandage (1968) as a possible optical counterpart of the hard X-ray transient source Cen

XR-2, although this identification was latter discarded. Because of its spectral characteristics, the object was then classified as a Wolf-Rayet star of type WN 7 (van der Hucht et al. 1981), while Vogt (1989) classified it as a nova-like variable. Diaz & Steiner (1995) – DS95 – showed that it is a binary system with an orbital period of 10.0 hr. The photometric orbital variation, determined by these authors, based on their spectroscopic observations, is approximately sinusoidal with an amplitude of ~ 0.3 mag. In spite of the period being relatively long (in the context of Cataclysmic Variables) it was not possible to identify

^{*} Based on observations made at Laboratório Nacional de Astrofísica/CNPq, Brazil, and at the 1.5m ESO telescope at La Silla, Chile.

[†] E-mail: alex@astro.iag.usp.br (ASO); steiner@astro.iag.usp.br (JES)

any spectral signature of the secondary star. A distance of 1400 pc was determined from the Na I D line equivalent width, and an $E(B - V) = 0.4 \pm 0.1$ was suggested from the average of three distinct determinations (4430 Å DIB and Na I D equivalent widths and He II 4686, 10124 Å lines ratio). Doppler tomography of WX Cen produced by DS95 suggests that the gas of the secondary has normal chemical abundance, while the wind of the primary star is probably over-abundant in helium ($\text{He}^{++}/\text{H} = 0.56$). DS95 also showed that, if the primary component of WX Cen is a white dwarf, then the secondary should have a mass below $0.35M_{\odot}$ and, therefore, be evolved. If, however, one assumes the hypothesis that the secondary is a main sequence star, it would have $M_2 = 1.16M_{\odot}$, and the primary, a mass of $M_1 > 3.5M_{\odot} \pm 0.5M_{\odot}$.

Steiner & Diaz (1998) included WX Cen in a group of 4 galactic binaries defined as the V Sge stars. The other three objects are V Sge (Herbig et al. 1965; Diaz 1999), V617 Sgr (Steiner et al. 1999; Cieslinski, Diaz & Steiner 1999) and DI Cru (Veen, van Genderen & van der Hucht 2002). They are characterized by the presence of strong emission lines of O VI and N V. Besides, He II is at least two times more intense than $\text{H}\beta$. The V Sge stars are similar to the Compact Binary Supersoft Sources (CBSS), seen in the Magellanic Clouds, but not that frequent in the Galaxy. CBSSs are interpreted as suffering hydrostatic hydrogen nuclear burning on the surface of a white dwarf. This burning is due to the high mass-transfer rate, a consequence of the fact that the systems have inverted mass ratios (see Kahabka & van den Heuvel (1997) for a revision and references). Patterson et al. (1998) also considered the hypothesis of Galactic CBSS nature for the stars V Sge, T Pyx and WX Cen, established on their extremely blue colors, high luminosities, orbital light curves and highly excited emission line spectra.

In an observational program to search for galactic WR stars, Shara et al. (1999) rediscovered WX Cen as a new WN3, when this star received the WR 48c designation. In our search for V Sge type stars, we selected WR 48c as a candidate, on the basis of spectroscopic criteria, for a detailed observational study. We, then, realized that WR 48c was the already known star WX Cen.

2 OBSERVATIONS

We observed WX Cen photometrically for 9 nights on 2000 April and 2003 May and July with the Boller & Chivens 60 cm and Zeiss 60 cm telescopes at the Pico dos Dias Observatory – MCT/LNA – located in Brazópolis, Southeast Brazil (see Table 1). A thin back-illuminated EEV CCD 002-06 chip and a Wright Instruments thermo-electrically cooled camera were employed to obtain the images. The timing was provided by a Global Positioning System (GPS) receiver. The frames were obtained through the Johnson V filter, with exposure times of 40, 50 and 80 seconds. We also observed this star in white light with 2 seconds exposure time, for which we used the same CCD, operated in the frame transfer mode, resulting in dead time between integrations of the order of milliseconds. Bias and flatfield exposures were obtained for correction of the stellar images. The images, except the ones obtained in frame transfer mode, present an

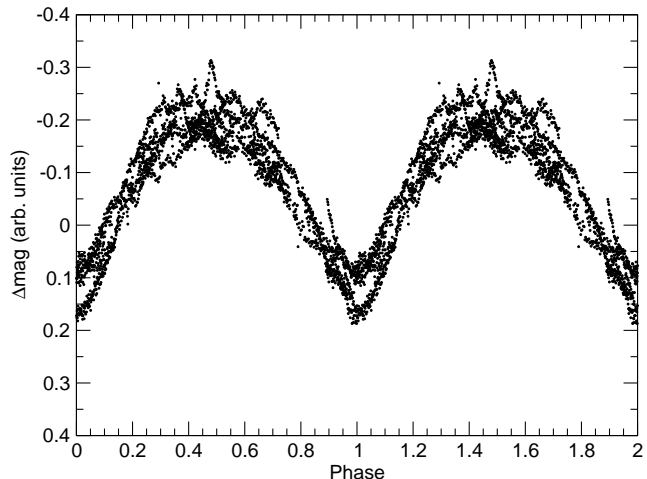


Figure 1. Average V light curve of the data obtained in 2000, folded with the orbital period and epoch from the photometric ephemeris.

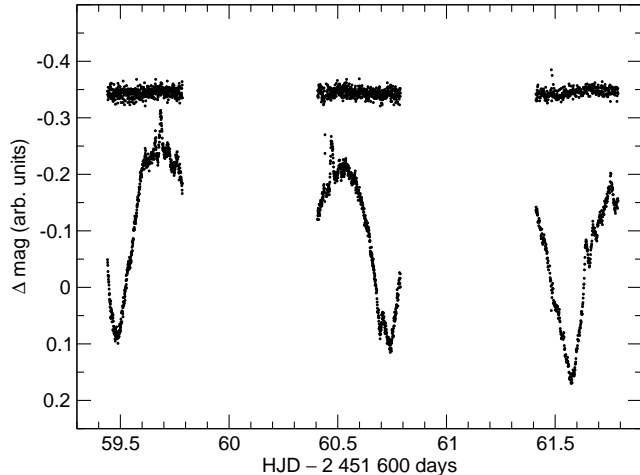


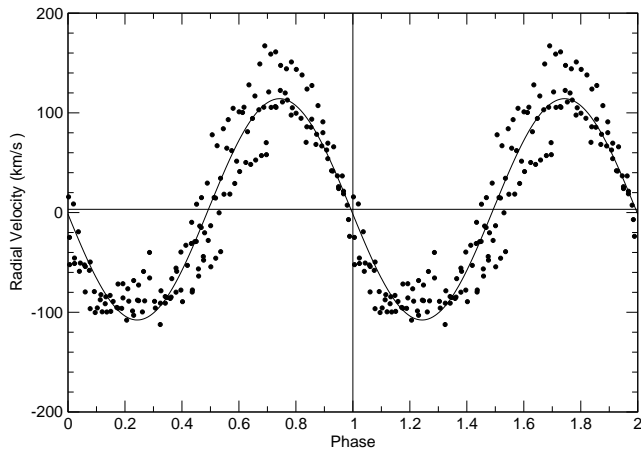
Figure 2. The light curve of WX Cen for the nights 2000 April 24, 25 and 26. The upper light curves are of the comparison star. An increase of 0.08 mag in the mean magnitude is seen in consecutive nights.

overscan region used for the CCD's zero point correction. The data reduction was performed with the standard procedures, using IRAF¹ routines. The star is located in a quite rich field; we, therefore, carried out differential PSF (Point Spread Function) photometry of WX Cen and four comparison stars of the field using the LCURVE package, written and kindly provided by M.P. Diaz. It makes use of

¹ IRAF is distributed by the National Optical Astronomy Observatories, which are operated by the Association of Universities for Research in Astronomy, Inc., under cooperative agreement with the National Science Foundation.

Table 1. Journal of photometric observations of WX Cen.

Date (UT)	Telescope	Number of exps.	Exp. time (s)	Filter
2000 Apr 07	Zeiss	461	40	V
2000 Apr 08	Zeiss	386	40	V
2000 Apr 09	Zeiss	492	40	V
2000 Apr 24	B&C	507	50	V
2000 Apr 25	B&C	555	50	V
2000 Apr 26	B&C	372	80	V
2003 May 20	Zeiss	327	50	V
2003 May 21	Zeiss	590	50	V
2003 Jul 02	Zeiss	5299	2	clear


Figure 3. He II 4686Å radial velocity curve, folded with the period and epoch given in the spectroscopic ephemeris. The sinusoidal curve fitted to the data has amplitude of 111 km s^{-1} .

DAOPHOT routines to treat automatically long time series data.

We also observed the object with the Cassegrain spectrograph coupled to the 1.6 m Boller & Chivens telescope at LNA on 2000 March. We used a dispersion grating with 900 lines per mm, covering the spectral range from 3700Å to 4950Å to obtain spectra with exposure times of 10 minutes (see Table 2). A thin back-illuminated SITe SI003AB 1024x1024 CCD was used as detector. Bias and dome flat-field exposures were obtained for correction of the CCD read-out noise and sensitivity. The width of the slit was adjusted to the conditions of the seeing. We took exposures of calibration lamps after every third exposure of the star, in order to determine the wavelength calibration solution. The image reductions, spectra extractions and wavelength calibrations were executed with IRAF standard routines.

An additional spectroscopic observation was made with the FEROS (Fiber-fed Extended Bench Optical Spectrograph - see Kaufer et al. (1999)) spectrograph at the 1.52 m telescope of ESO (European Southern Observatory) in La Silla, Chile, on 2002 January 24. The FEROS spectrograph uses a bench mounted Echelle grating with reception fibers in the Cassegrain focus. It supplies a resolution of $R = 48\,000$, corresponding to 2.2 pixels of $15 \mu\text{m}$, and spectral coverage from 3600Å to 9200Å. A completely automatic

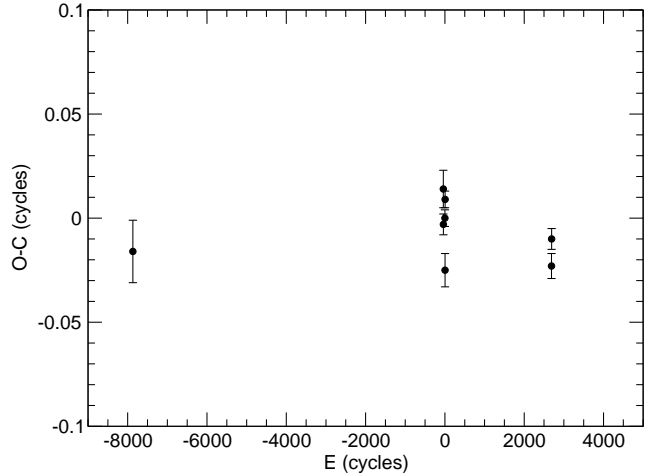

Figure 4. The O–C diagram corresponding to the photometric ephemeris. The first point (cycle –7869) is the timing of the minimum of the continuum modulation presented by DS95. The other points are the timings of minima measurements from the photometric data presented in this work (see Table 3).

Table 2. Journal of spectroscopic observations of WX Cen.

Date (UT)	Instrum.	Number of exps.	Exp. time (s)	Resolution (Å)
2000 Mar 12	Cass.	6	600	2.8
2000 Mar 24	Cass.	53	600	2.8
2000 Mar 25	Cass.	54	600	2.8
2000 Mar 26	Cass.	54	600	2.8
2002 Jan 24	FEROS	1	1800	0.1

on-line reduction system is available and was adopted by us. We obtained a single spectrum with integration time of 30 minutes.

3 DATA ANALYSIS

3.1 The optical light curve

The average light curve of WX Cen (Fig. 1) displays a well defined orbital modulation with total amplitude of approximately 0.32 magnitudes. It is asymmetric, and can not be adjusted by a simple sine wave. The maximum is wider and the minimum, narrower than the expected from a sine wave. The rise is also faster than the fall to the minimum. This light curve has a minimum with a shape that resembles the ones of V Sge and of V617 Sgr as well as the galactic CBSS QR And. Superposed on it, there is a fluctuation with time-scale of tens of minutes. In addition to this fast fluctuation, there is a variation with time-scale of one day and with approximately 0.08 mag, as can be seen in the light curves of the nights of 2000 April 24, 25 and 26 (Fig. 2). Single flare-like events with amplitude of 0.08 magnitudes and lasting for about 30 minutes are also seen (see Fig. 2).

We searched the data for optical pulsations in the range of 10 to 200 cycles day⁻¹. No periodic signal is seen but power excess with $T \sim 85$ cycles day⁻¹ (17 min) is visible. This is to be compared to the 17–27 min oscillations, seen in V617 Sgr (Steiner et al. 1999) and to the 60 min oscillations, seen in V Sge (Herbig et al. 1965). In addition, a power law signal with

$$\text{Log } P = \alpha \log f + C \quad (1)$$

is seen, where $\alpha = -1.85 \pm 0.04$. This is the classical signature for low frequency flickering.

In order to estimate the inclination of the system, we will compare the light curve of WX Cen with that of QR And. From the observed amplitude of the light curve of QR And, which varies from $\Delta m = 0.25$ magnitudes (Meyer-Hofmeister et al. 1998) to $\Delta m = 0.5$ magnitudes (McGrath et al. 2001), an inclination of $i = 55^\circ$ was derived (Meyer-Hofmeister et al. 1998). As the observed light curve amplitude of WX Cen is within the observed range for QR And, and as the overall light curve shape and photometric behavior are similar, we will adopt $i = 55^\circ$ for WX Cen as well.

3.2 Refining the orbital period

The orbital radial velocity curve obtained from the He II 4686Å line is shown in Fig. 3. The spectroscopic ephemeris associated to this radial velocity curve is

$$T_{(spec)}(HJD) = 2\,451\,659.544(\pm 17) + 0.416\,961\,5(\pm 22) \times E(2)$$

This ephemeris was calculated defining the zero phase as the crossing from positive to negative values of the radial velocities when compared to the systemic velocity, $\gamma = 3$ km s⁻¹. We refined the spectroscopic period from the value determined by DS95, as the number of orbital cycles elapsed from their zero phase timing to the present one is long enough, that is, 7870 cycles.

The ephemeris of the light curve minima is

$$T_{(min)}(HJD) = 2\,451\,659.485(\pm 13) + 0.416\,960\,1(\pm 28) \times E(3)$$

The value of the photometric period presented in this ephemeris was determined from the (O–C) diagram shown in Fig. 4, which was in turn constructed from the measurements presented in Table 3. The orbital period derived from the radial velocities and from the photometric minima are the same, within 1σ confidence level. The delay between the spectroscopic ephemeris and what is expected from the photometric one is about $\Delta\phi = 0.14$ and is similar to what is reported in DS95.

3.3 The high-resolution spectrum

As the high resolution spectrum was obtained with a 1.5 m telescope, it is quite noisy. Even so, we can identify a number of lines and obtain profile information (Table 4). The most intense hydrogen (H α , H β) and helium (4686Å) lines present a structure with three peaks. One, near rest wavelength, at about +10 km s⁻¹, and two side-peaks, with velocities of -180 km s⁻¹ and +240 km s⁻¹ (see Table 5 and Fig. 5).

Most of the lines can be identified with the transitions from the Balmer series, He II lines, C III, C IV, N III, N

Table 3. Times of photometric minima.

Date (UT)	Observed Minimum (HJD)	E (cycles)
1991 Apr 31	2 448 378.410 (± 15)	-7869
2000 Apr 07	2 451 642.821 (± 9)	-40
2000 Apr 08	2 451 643.638 (± 5)	-38
2000 Apr 24	2 451 659.485 (± 4)	0
2000 Apr 25	2 451 660.711 (± 8)	3
2000 Apr 26	2 451 661.579 (± 4)	5
2003 May 20	2 452 780.668 (± 6)	2689
2003 May 21	2 452 781.515 (± 5)	2691

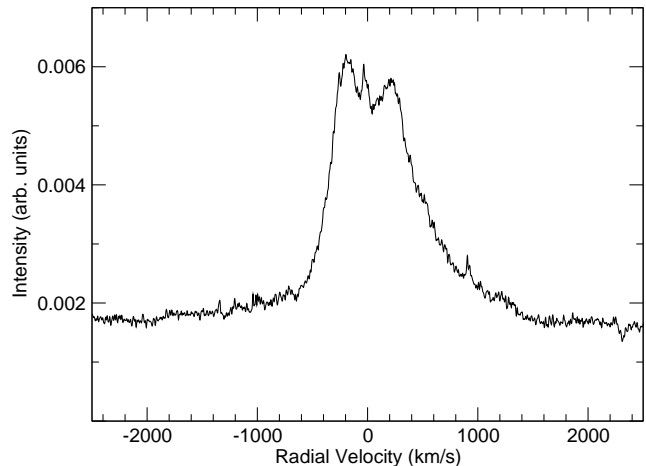


Figure 5. High resolution spectrum of H α , showing its multiple peaks.

V, O III, O V and O VI (see Table 4). But there are a few emission lines that are not generally seen in the context of Cataclysmic Variables or WR stars. We believe that they are spurious FEROS artifacts that appear in faint targets. There is no evidence of He I lines (see Table 4).

Another important feature in the high-resolution spectrum is the very high velocity associated to the extended red wing seen in the strongest Balmer and He II lines.

There are two additional points that deserve consideration. First, the high range of ionization of oxygen, which varies from O III to O VI (see Section 4.2). The second point is the absence of N IV emission, besides its analog of O V being clearly present.

3.4 The medium-resolution spectrum

In our medium-resolution spectra we see an unexpected phenomenon: on several occasions, absorptions are present in the Balmer lines blue wings, and this event is quite variable. Fig. 6 illustrates the average spectra with and without the presence of such absorptions. In Fig. 7 we show the ratio of the average spectrum with absorption to the average spectrum without absorption. We clearly see the phenomenon.

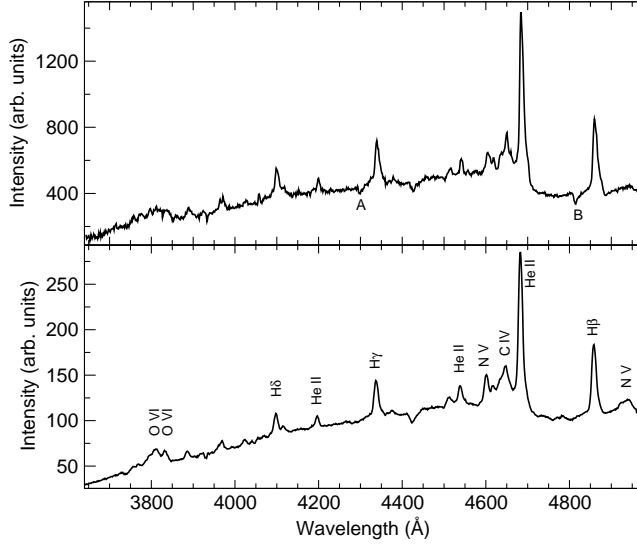


Figure 6. Average medium resolution spectrum of WX Cen with the absorptions (labelled A and B, top spectrum) and without the absorptions (bottom spectrum).

Table 4. Line identification in WX Cen: High-resolution spectrum.

Identif.	λ_{obs} (Å)	$-W_{\lambda}$ (Å)	FWHM (km s ⁻¹)
Emission lines:			
He II/H δ +N III	4101.8	7	700
He II/H γ	4341.3	9	900
N III	4515
He II	4539.6	12	1060
N V	4607.8	5	700
N V	4625.9	3	840
N III	4640	3	700
C III	4650
C III+C IV	4664.1	3	450
He II	4687.1	13	700
He II/H β	4863.2	15	860
O V	4930
N V	4944
O V	5115.7	2	300
He II	5413.4	5	670
O V	5580
O III	5592
O V	5600
C IV	5806.2	7	670
C IV	5817.7	2	260
He II/H α	6563.8	44	820
Absorption features:			
Ca II	3933.49	-0.76	66
Ca II	3968.18	-0.38	27
DIB	5780.18	-0.56	129
Na I	5889.66	-0.87	40
Na I	5895.67	-0.74	37

Table 5. Velocities of the multiple peaks of emission lines, relative to the rest wavelengths.

	peak 1 (km s ⁻¹)	peak 2 (km s ⁻¹)	peak 3 (km s ⁻¹)
He II 4686Å	-161	+24	+237
H β	-186	-13	+259
He II 5411Å	-176	+57	+233
C IV 5801Å	-59 :	+10:	+269
H α	-185	-21	+219

Table 6. Line properties from medium-resolution spectrum.

Identif.	λ_{obs} (Å)	$-W_{\lambda}$ (Å)	FWHM (km s ⁻¹)
Emission lines:			
O III	3755-91
O VI	3813.5
O VI	3835.6
He II/H ϵ	3889.1	1.5	800
He II	4025.5	0.9	790
He II/H δ	4101.2	4.8	...
He II	4199.0	1.7	...
He II/H γ	4340.8	4.4	747
N III	4515.3	1.1	963
He II	4541.6	1.9	713
N V	4604.0	3.1	730
N V	4618.7	1.6	838
C III-C IV/N III	4648.8	10.0	2000
He II	4685.9	17.6	723
He II/H β	4861.9	9.8	765
Absorption features:			
DIB	4428.6	-1.7	...
Ca II	3933.4	-0.4	...

The absorption occurs at -2880 km s⁻¹ in H β and -2840 km s⁻¹ in H γ . We see, at the same time, an emission in the bluest part of H β , at the velocity of -3500 km s⁻¹. Evidence of a weak emission at $+3500$ km s⁻¹ in H β is also seen.

Significant long-term variability in the line intensities and line ratios seems to be visible in spectra from distinct epochs. In table 1 from Steiner & Diaz (1998) one can see the equivalent widths of H α , H β and He II 4686Å as 61Å, 15Å and 37Å. From our high-resolution spectra (Table 4), we have, respectively, 37.0Å, 13.8Å and 12.2Å. Not only the lines seem to be much weaker but also the H β /He II ratio is much higher. This can easily be seen by comparing Fig. 6 with fig. 1 in Steiner & Diaz (1998). From our medium resolution spectra (Table 6), we can see that the intensity H β /He II ratio is again reversed with respect to our high resolution spectrum, although H β is even weaker.

The lines also seem to be significantly narrower in the observations of the years 2000 and 2002 when compared to the observations of 1991 (DS95). While in 1991 the FWHM of the emission lines was typically 1100 km s⁻¹, the latest observations show FWHM of about 700 km s⁻¹. Even considering that the data were obtained with distinct instruments and different resolution, this difference seems to

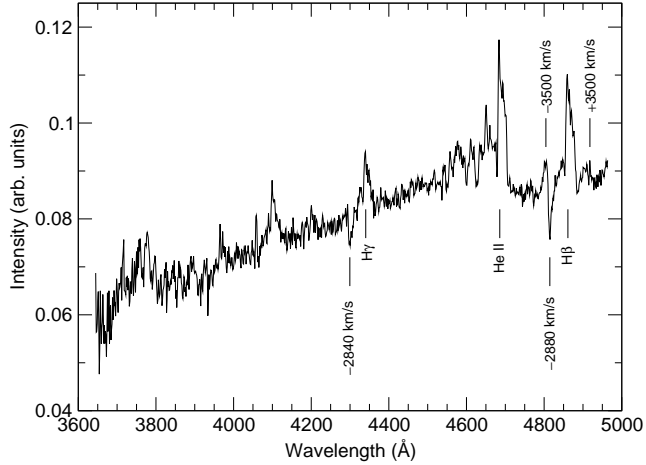


Figure 7. Average medium resolution spectrum of WX Cen with absorption divided by the average spectrum without absorption.

be significant. This suggests that in recent years the observations were made with the system in a less active state.

We have compiled all the lines observed in this object so far. These lines are shown in Table A1, in which we list the lines for similar terms from the relevant CNO ionization species.

Fig. 8 shows the variation of the equivalent width as a function of time. It peaks at spectroscopic phase zero. This is quite similar to what has been reported for V617 Sgr (Cieslinski, Diaz & Steiner 1999). The interpretation of this curve is quite straightforward: most of the eclipsed continuum comes from the heated surface of the secondary star (mass donor) while the He II line is emitted in a non-eclipsed region (disc/wind/rim).

3.5 The Temporal Variance Spectrum – TVS

In an attempt to examine the line variability in more detail we performed the Temporal Variance Spectrum – TVS – analysis. In this procedure the temporal variance is calculated, for each wavelength pixel, from the residuals of the continuum normalized spectra to the mean spectrum. For further details and discussions of this method, see Fullerton, Gies & Bolton (1996). The observed median resolution (Cassegrain) mean spectrum of WX Cen and the calculated TVS are shown in Figs. 9 and 10. A noticeable feature present in the N V 4603-19Å and He II emission lines is the double-peaked line profile, resulting not from a true line profile variation – lpv – but from a radial velocity variation due to the binarity. This phenomenon is described in Fullerton, Gies & Bolton (1996) (see their fig. 1). In this case we expect $\sigma/I \sim K/FWHM$, where σ is the TVS line variance and I is the related observed line intensity. The ratio σ/I is 14 per cent for H β and 12 per cent for He II 4686Å. These values of σ/I are not an intrinsic property, but an artifact from the TVS analysis.

The TVS of WX Cen also shows clear evidence of the

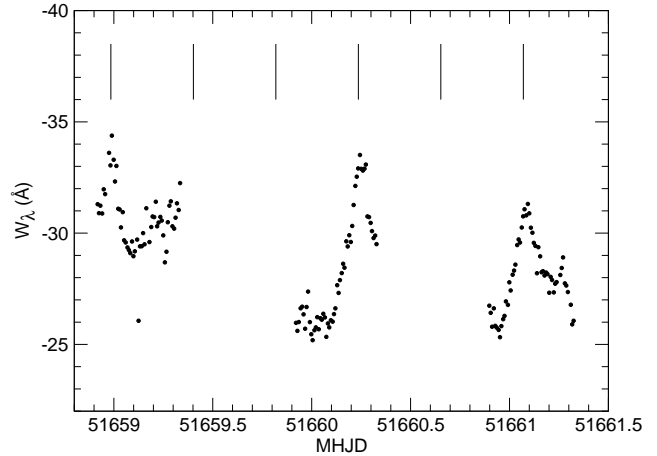


Figure 8. He II 4686Å equivalent width measurements from the nights of 2000 March 24, 25 and 26. The vertical lines represent the timings of crossing from positive to negative values of the radial velocities when compared to the system velocity, as defined in the spectroscopic ephemeris.

variable absorptions in the blue wings of the Balmer lines. There are two peaks, one with velocity of -2900 km s^{-1} and other with -3500 km s^{-1} , which correspond to the absorption and emission peaks near H β , respectively (see Fig. 7). Besides, the O VI 3811/34Å lines show strong variability in the red wings, with a displacement of approximately 700 km s^{-1} relative to the rest wavelength. The red wings of the Balmer and He II lines show strong variability that extends to velocities up to 1500 km s^{-1} . This variability of the O VI lines, for instance, indicates that there are two emitting regions. One, with low variability, has normal velocity and another, highly variable, has high and positive velocity.

4 DISCUSSION

4.1 The hydrogen content

One way of analysing the presence/absence of hydrogen in a strong helium emitting spectrum is by comparing the He II 4859Å+H β to the geometric mean of the two adjacent transitions of the He II Pickering series. This criterion has been widely used, for instance, by Smith, Shara & Moffat (1996) in defining their three dimensional classification of WN stars. We define a Pickering parameter, p , such that

$$p = \frac{I(4859\text{Å} + 4861\text{Å})}{[I(4541\text{Å}) \times I(5411\text{Å})]^{1/2}} \quad (4)$$

For a pure He II spectrum one expects $p = 1$ (SSM96). Any value of p larger than 1 would mean hydrogen in the object. In the case of WX Cen, the measured value is about $p = 3.1$.

In case both hydrogen and helium lines were optically thin, it would be easy to determine the relative abundance between the two species. In this case (Conti, Leap & Perry 1983):

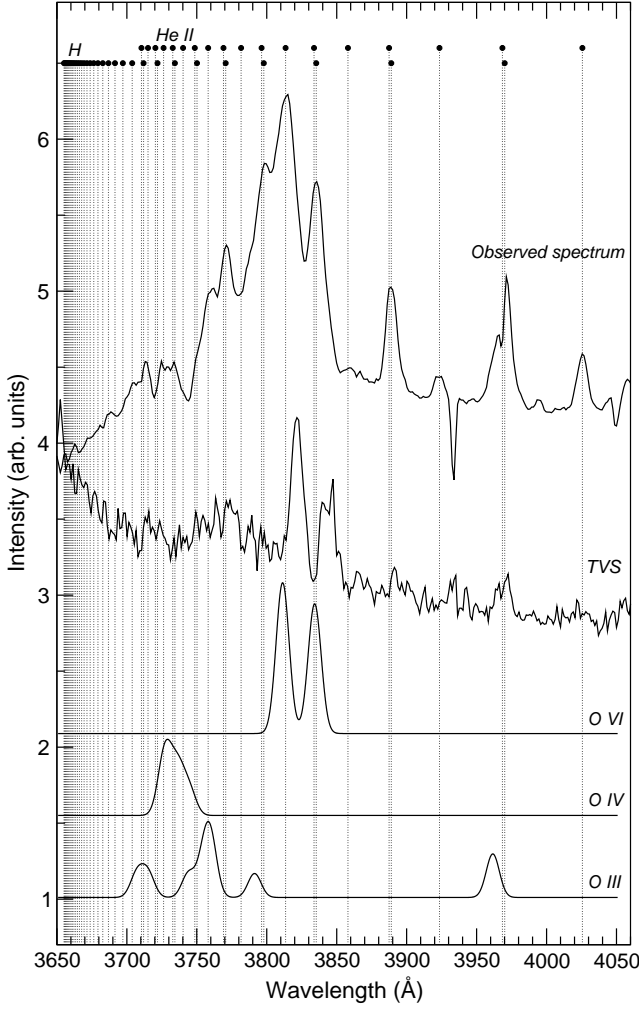


Figure 9. Intensity (observed) spectrum, TVS, and synthetic spectra for O VI, O IV and O III, from 3650Å to 4050Å. Also shown (as vertical dotted lines) are the positions of the Pickering and Balmer series lines.

$$\frac{N(H^+)}{N(He^{++})} = p - 1 \quad (5)$$

and the abundance would be $N(H^+)/N(He^{++}) \sim 2.1$.

The largest uncertainty in this determination comes from the hypothesis that all of the involved lines are optically thin.

For the optically thick case, one gets (see Conti, Leap & Perry (1983))

$$\frac{N(H^+)}{N(He^{++})} = p^{3/2} - 1 \quad (6)$$

which, for WX Cen, gives $N(H^+)/N(He^{++}) \sim 4.5$. With a high resolution spectrum as is the present case, however, we can determine the relative abundance using intensities at a given velocity in the profile, in which we can be reasonably secure that the lines are optically thin. For instance, if we use the intensity in the red wing that corresponds to, say, 300 km s⁻¹, we may be in such a situation. Defining a parameter $y(v)$, so that

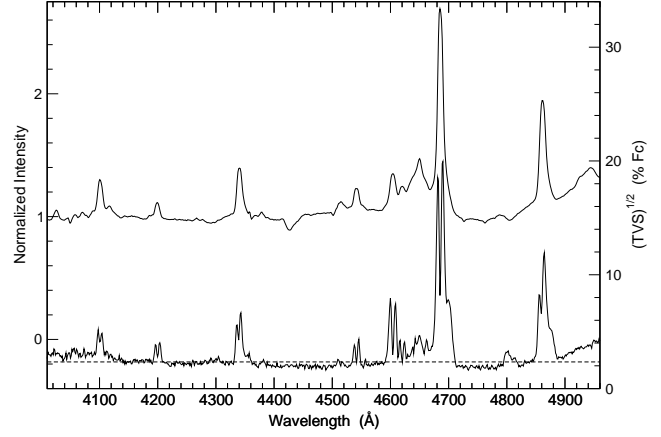


Figure 10. Intensity spectrum (above) and TVS (below) of WX Cen from 4010Å to 4950Å. The TVS ordinate (right axis) gives the amplitudes as percentage of the normalized continuum. The TVS statistical threshold for $p = 1\%$ is represented by the dashed line.

$$y(v) = \frac{I_{4861\text{\AA}}(v) - [I_{4541\text{\AA}}(v + dv) \times I_{5411\text{\AA}}(v + dv)]^{1/2}}{[I_{4541\text{\AA}}(v) \times I_{5411\text{\AA}}(v)]^{1/2}} \quad (7)$$

where $I_{4861\text{\AA}}(v)$ is the intensity of the line at velocity v from the rest wavelength of H β , $I_{5411\text{\AA}}(v + dv)$ is the intensity of the line at velocity $v + dv$ from the He II 5411Å rest wavelength. The H^+/He^{++} abundance can be estimated as

$$\frac{N(H^+)}{N(He^{++})} = y \quad (8)$$

In the case of WX Cen the parameter y was measured at $v = 300$ km s⁻¹ while $dv = 122$ km s⁻¹. We found $N(H^+)/N(He^{++}) \sim y \sim 2.3$. This is to be compared with the range found by DS95: $N(H^+)/N(He^{++}) \sim 1.7$ to 7.

In the Smith, Shara & Moffat (1996) three dimensional classification scheme for WN stars, one could classify WX Cen spectroscopically as WN3hpec, where the pec suffix indicates, like in DI Cru, the presence of strong O VI emission lines. It is clear, however, that we do not consider WX Cen as having WR nature.

4.2 CNO abundance

An unusual characteristic we observe in the spectrum of WX Cen is the large range of ionization degree. At the same time we see O VI emission, we also see O V, O IV and O III (Table A1). This is very different from what is seen, for example, in WR stars. In these systems the wind and ionizing photons have similar dilution factors and the ionization parameter is constant to a first approximation. Yet in V Sagittae stars one expects a wind, accretion disc, hot spot, rim, spill-over and a secondary star. The range of ionization parameter in each of these regions can be very distinct. The expected range of ionization species in V Sge objects should, therefore, be larger than in WR stars. Herbig et al. (1965) also observed O III and O VI in V Sge.

Is the N/O ratio anomalous in WX Cen? Why do we see O V but not the same transition in N IV? From the intensity ratios, we obtain $N/O < 0.1$. This is similar to Planetary

Nebulae of type II or to the solar abundance but is quite distinct from WN stars ($N/O \sim 20$ to 50)

4.3 The distance to the system

DS95 made a distance determination on the basis of the diffuse interstellar band –DIB– at 4430\AA , interstellar Na D lines and the decrement of He II lines and found a distance of about 1.4 kpc. To measure the equivalent width of the 4430\AA band is difficult, given that it is hard to define the nearby continuum, and the Na D lines are saturated (Fig. 11). We will, therefore, revisit this issue. Let's first estimate the interstellar extinction from the diffuse interstellar bands. The DIBs and reddening have been calibrated by many authors. From Herbig (1975), we have

$$E(B - V) = W_\lambda(4430\text{\AA})/2.3 \text{ mag} \quad (9)$$

This is different from the relation in Allen (1973), used by DS95, by about a factor of 2. We found $W_\lambda(4430\text{\AA}) = 1.7$ (Table 6), and obtain $E(B - V) = 0.74$.

The most reliable DIB for evaluating the interstellar extinction in the case of WX Cen seems to be the 5780\AA feature. We measured an equivalent width of $W_\lambda = 0.56 \pm 0.01\text{\AA}$. Somerville (1988) gives the following relation between its equivalent width and color excess

$$E(B - V) = (W_\lambda(5780\text{\AA}) + 46)/940 \quad (10)$$

where W_λ is given in mÅ. In the case of WX Cen we have $E(B - V) = 0.63$ and we will adopt this as the color excess. This is about 50 per cent larger than the value estimated by DS95. From a calibration of the color excess *versus* distance, obtained both for open clusters (Dias, Lépine & Alessi 2002) and field stars (see Table A2), we derive a distance of about 2.8 ± 0.3 kpc.

The Na I lines for WX Cen and stars in its field (Franco 2000) have velocities, in LSR, that are listed in Table 7. Four absorption systems can be identified and we will call these components from 1 to 4.

From the other stars in the field of the Coalsack, observed by Franco (2000), one concludes that the distance to WX Cen has to be well in excess of 800 pc. The numbers in Table 7, as well as the equivalent widths of the absorption components 2 and 3, suggest a distance of about 1.8 to 2.7 kpc which seems to be consistent with the value derived above.

The absolute magnitude is, then, of about $M_V = -0.5$ and color $(B - V)_0 = -0.2$.

4.4 Spill-over; SN Ia precursor?

A somewhat striking characteristic of the spectrum of WX Cen are the red wings in the emission lines, seen in the high resolution spectrum, extending to about $+1300 \text{ km s}^{-1}$. This is similar to what was observed by Cieslinski, Diaz & Steiner (1999) in V617 Sgr. In the Doppler diagram presented by these authors, after subtracting the symmetric profile, one can notice a high velocity component extending to $V \sim -800$ to -1000 km s^{-1} , both in V_x and in V_y . In addition there is a strong emission concentrated at $V_x \sim -200 \text{ km s}^{-1}$. Steiner et al. (1999) explained these characteristics by assuming that the -200 km s^{-1} component is due

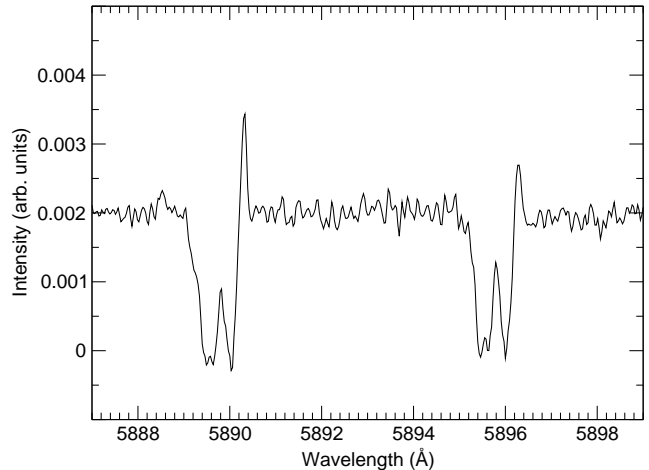


Figure 11. Na I interstellar absorption lines. The red wing emissions are due to bad sky subtraction.

to the high disc rim, similar to the ones observed in CBSSs (Meyer-Hofmeister, Schandl & Meyer 1997). The high velocity component was explained in V617 Sgr as a consequence of spill-over gas, following ballistic trajectories and closely approaching the white dwarf. Such a configuration would explain the red wing characteristic if the high resolution spectrum was taken at a phase immediately before the photometric minimum. This is indeed the case. The central exposure of the high resolution spectrum was at photometric phase 0.787. We predict that at opposite phase the wing should be to the blue. This phenomenon is also likely to be variable as there is no hint of such a component in the Doppler diagram presented in DS95.

A puzzling feature still remains unexplained. The TVS spectrum shows a highly variable component in the highly ionized species O VI. This component is seen at $V \sim 700 \text{ km s}^{-1}$. This component is also seen in the TVS red wings of H β and He II 4686\AA . We have no explanation for this.

The satellite-like events at the Balmer lines, being interpreted as due to ejected gas, are consistent with the idea that the compact star is a white dwarf. With an orbital inclination of $i = 55^\circ$, and observed velocity of 3500 km s^{-1} , we derive the intrinsic velocity of the "jet" as $V = 6100 \text{ km s}^{-1}$. This corresponds to the escape velocity of a white dwarf with a mass of $M \sim 0.9M_\odot$. With the high accretion rate ($dM_1/dt \sim 10^{-7}M_\odot \text{ year}^{-1}$) required in order to have surface nuclear burning (Kahabka & van den Heuvel 1997), this white dwarf may reach the Chandrasekhar limit and become a SN Ia on a time-scale of 5×10^6 years.

CBSSs have been considered as possible candidates to SN Ia precursors (Hachisu et al. 1999). These authors have shown a channel to SN Ia by evolving a helium rich Supersoft X-ray binary. Hachisu & Kato (2003) also showed that V Sge may become a SN Ia.

5 CONCLUSIONS

The main conclusions of this paper are:

- (i) We confirmed the orbital period of WX Cen de-

Table 7. Radial velocities (km s⁻¹) of Na ID absorption components and distances (kpc).

Component	WX Cen	SAO252025	SAO252085	SAO252146	Coalsack
1	-4.1	-0.8	-3.5	-4.8	-2/-4
2	-23.9	-26.6	-21.6	-23.8	...
3	-32.0	-37	-33.1	-35.1	...
4	-39.0		-42
distance	...	1.81	2.48	2.72	0.2

terminated by DS95 and refined its value to $P_{orb} = 0.416\,961\,5(\pm 22)$ d, based on spectroscopic observations.

(ii) The light curve has total amplitude of approximately 0.32 magnitudes and is non-sinusoidal in the sense of having a narrow, V-shaped, minimum. The object presents flickering with time-scales of tens of minutes. Night-to-night variations of about 0.08 mag are also observed.

(iii) We identified most of the emission lines as due to Balmer, He II, C IV, N V, O III, O V, O VI.

(iv) The object shows absorption satellites in the Balmer lines with $V = -2900$ km s⁻¹ and in emission with $V = \pm 3500$ km s⁻¹. These highly variable events remind the satellites in emission in CBSS.

(v) The analysis of the emission lines show that the He II 4686Å line became weaker between 1991 and 2000/2002 observations. At the same time the emission lines were narrower, suggesting that in 2000/03 the system was in a less active state than in 1991.

(vi) The object presents red-shifted emission in high ionization species. Extended red wing emission is also seen in the strongest lines. The O VI lines show strong variability with velocity of about 700 km s⁻¹.

(vii) An analysis of the He II Pickering series decrement shows that the system has significant amount of hydrogen, with an abundance, by number, between 2.1 and 4.5.

(viii) We estimate the color excess as $E(B - V) = 0.63$ on the basis of the observed DIB at 5780Å. Given the distance-color excess relation in the direction of WX Cen, this implies a distance of 2.8 ± 0.3 kpc. Interstellar absorption of the Na I D lines show components at -4.1 km s⁻¹, which corresponds to the velocity of the Coalsack, and three other components a -23.9 , -32.0 and -39.0 km s⁻¹. These components are also seen with similar strengths in field stars that have distances between 1.8 and 2.7 kpc. The intrinsic $B - V$ color index of WX Cen is $(B - V)_0 = -0.2$ and the absolute magnitude, $M_V = -0.5$.

(ix) A possible explanation for the extended wings in the strong emission lines is that the system has a spill-over stream similar to what is seen in V617 Sgr. We predict that when observed in opposite phase, blue wings would be observed.

(x) The velocity of the satellites is consistent with the idea that the central star is a white dwarf with a mass of $M \sim 0.9M_\odot$. With the high accretion rate, it may become a SN Ia in a time-scale of 5×10^6 years.

REFERENCES

- Allen C. W., 1973, *Astrophysical Quantities*. Athlone, London
- Cieslinski D., Diaz M. P., Steiner J. E., 1999, *AJ*, 117, 534
- Conti P.S., Leep E.M., Perry D.N., 1983, *ApJ*, 268, 228
- Dias W. S., Lépine J. R. D., Alessi B. S., 2002, *A&A*, 388, 168
- Diaz M. P., 1999, *PASP*, 111, 76
- Diaz M. P., Steiner, J. E., 1995, *AJ*, 110, 1816
- Eggen O. J., Freeman K.C., Sandage, A., 1968, *ApJ*, 154, L27
- Franco G.A.P., 2000, *MNRAS*, 315, 611
- Fullerton A.W., Gies D.R., Bolton C.T., 1996, *ApJ Supp*, 103, 475
- Hachisu I., Kato M., Nomoto K., Umeda H., 1999, *ApJ*, 519, 314
- Hachisu I., Kato M., 2003, preprint (astro-ph/0308065)
- Herbig G.H., 1975, *ApJ*, 196, 129
- Herbig G. H., Preston G. W., Smak J., Paczynski B., 1965, *ApJ*, 141, 617
- Kahabka P., van den Heuvel E. P. J., 1997, *ARA&A*, 35, 69
- Kaufer A., Stahl S., Tubbesing S., Norregard P., Avila G., François P., Pasquini L., Pizzella A., 1999 *The Messenger*, 95, 8
- McGrath T. K., Schmidtke P. C., Cowley A. P., Ponder A. L., 2001, *AJ*, 122, 1578
- Meyer-Hofmeister E., Schandl S., Meyer F., 1997, *A&A*, 321, 245
- Meyer-Hofmeister E., Schandl S., Deufel B., Barwig H., Meyer F., 1998, *A&A*, 331, 612
- Patterson J. et al., 1998, *PASP*, 110, 380
- Shara M. M., Moffat A. F. J., Smith L. F., Niemela V. S., Potter M., Lamontagne R., 1999, *AJ*, 118, 390
- Smith L. F., Shara M. M., Moffat A. F. J., 1996, *MNRAS*, 281, 163
- Somerville W. B., 1988, *MNRAS*, 234, 655
- Steiner J. E., Diaz M. P., 1998, *PASP*, 110, 276
- Steiner J. E., Cieslinski D., Jablonski F. J., Williams R. E., 1999, *A&A*, 351, 1021
- van der Hucht K.A., Conti P.S., Lundstrom I., Stenholm B., 1981, *Space Sci. Rev.*, 28, 227
- Veen P. M., van Genderen A. M., van der Hucht K. A., 2002, *A&A*, 385, 619
- Vogt N., 1989, in *Classical Novae*, ed. Bode & Evans, p. 225

APPENDIX A:

Table A1. The CNO emission line table for WX Cen.

	O		N		C	
	O III					
IP (eV)	54.94					
Term	$\lambda(\text{\AA}) - W_\lambda \text{ (\AA)}$					
$3s\ ^1P^0 - 3p\ ^1P$	5592	y ^a				
$3s\ ^3P^0 - 3p\ ^3D$	3760	y				
	3755	y				
	3757	y				
	3791	y?				
	O IV		N III			
IP (eV)	77.41		47.45			
Term	$\lambda(\text{\AA}) - W_\lambda \text{ (\AA)}$		$\lambda(\text{\AA}) - W_\lambda \text{ (\AA)}$			
Doublets						
$3s\ ^2S - 3p\ ^2P^0$	3063	...	4097	bl		
	3072	...	4103	...		
$3s\ ^2P^0 - 3p\ ^2D$	3349	...	4200	bl		
	3348	...	4196	...		
	3378	...	4216	...		
$3p\ ^2P^0 - 3d\ ^2D$	3412	...	4641	y		
	3404	...	4634	y		
	3414	...	4642	y?		
Quadruplets						
$3s\ ^4P^0 - 3p\ ^4D$	3386	...	4515	1.1		
	3381	...	4511	...		
$4p\ ^2D - 4d\ ^2P^0$	7716			
$5f\ ^2F^0 - 6g\ ^2G$	8019	...		
	O V		N IV		C III	
IP (eV)	113.90		77.47		47.89	
Term	$\lambda(\text{\AA}) - W_\lambda \text{ (\AA)}$		$\lambda(\text{\AA}) - W_\lambda \text{ (\AA)}$		$\lambda(\text{\AA}) - W_\lambda \text{ (\AA)}$	
Singlets						
$3s\ ^1S - 3p\ ^1P^0$	5114	y	6381	...	8500	...
Triplets						
$3s\ ^3S - 3p\ ^3P^0$	2781	...	3479	...	4647	10:
	2787	...	3482	...	4650	...
	2790	...	3484	...	4651	...
$3s\ ^3P^0 - 3p\ ^3P$	2731	...	3463	...	4666	2.3:
	2744	...	3461	...	4673	...
	2729	...	3475	...	4663	...
$3p\ ^3P^0 - 3d\ ^3D$	5598	y	7123	np	9715	...
	5580	y	7109	np	9705	...
	5573	y	7103	np	9701	...
	5604	...	7127	...	9718	...

^a Meaning of the codes: y = line present; bl = blended line; np = line not present.

Table A1 – *continued*

	O		N		C	
	O VI		N V		C IV	
IP (eV)	138.12		97.89		64.49	
Term	$\lambda(\text{\AA}) - W_{\lambda}(\text{\AA})$		$\lambda(\text{\AA}) - W_{\lambda}(\text{\AA})$		$\lambda(\text{\AA}) - W_{\lambda}(\text{\AA})$	
$3s\ ^2S - 3p\ ^2P^0$	3811	y	4604	3.4	5801	3.9
	3834	y	4620	2.8	5812	2.4
$4s\ ^2S - 4p\ ^2P^0$	9342		11331	...	14335	...
	9398	...	11374	...	14362	...
(5-6)	2070	...	2981	...	4658	y?
(6-7)	3435	...	4945	y	7726	y
(6-8)	2083	...	2998	...	4685	bl
(7-8)	5291	y?	7618	y	11908	...
(7-9)	3143	...	4520	...	7063	y?
(8-9)	7715	y	11110	...	17368	...
(7-10)	2431	...	3502	...	5471	np
(8-10)	4494	...	6478	...	10124	...
(9-10)	11033	...	15536	...	24278	...
(8-11)	3427	...	4943	...	7737	y?
(9-11)	6202	...	8927	...	13954	...
(10-11)	14590	...	21000	...	32808	...

Table A2. Distance and color excess for open clusters and stars in the fields of WX Cen.

Name	<i>V</i>	<i>B-V</i>	<i>E(B-V)</i>	d (kpc)	Sp
Clusters					
Stock 16	0.49	1.64	...
Ruprecht 107	0.46	1.44	...
Collinder 271	0.29	1.17	...
Basel 18	0.51	2.23	...
NGC 4815	0.81	3.08	...
Trumpler 21	0.20	1.26	...
BH 144	0.60	9.35	...
Hogg 16	0.41	1.58	...
Collinder 272	0.47	2.04	...
Pismis 18	0.50	2.24	...
Stars					
114800	8.00	0.12	0.35	1.17	B2 IV NE
114737	8.01	0.17	0.46	2.00	O9 IV
114886	6.87	0.12	0.40	1.23	O9 IV
114478	8.68	0.49	0.65	3.21	B1 Ib
115034	8.80	0.09	0.35	1.90	B0.5 Vn
114122	8.57	0.59	0.73	3.10	B1 Iab
115363	7.79	0.61	0.74	3.20	B1 Ia
113754	9.50	0.63	0.90	4.43	O9.5 Ia
CP-623111	10.20	0.19	0.44	2.69	B1 V
CP-613512	10.03	0.35	0.58	3.34	B1 III
115071	7.96	0.24	0.50	1.03	B0.5 Vn
113432	8.86	0.80	0.91	2.35	B1 Ib
CP-632544	9.97	0.49	0.67	5.64	B1 Ib
CP-613598	10.3	0.84	0.96	6.40	B5 Iap
113411	9.05	0.46	0.71	2.72	O9.5 IV
WX Cen	13.6/14.2	0.4	0.63	2.9 ± 0.3	WN3h pec